Journal of Mechatronics, Electrical Power, and Vehicular Technology 17 (2026) 90-106

Journal of Mechatronics, Electrical Power, and Vehicular Technology

e-ISSN: 2088-6985
p-ISSN: 2087-3379

mev.brin.go.id

Fractional tent map-chaotic horse herd optimization for global MPPT under partial shading conditions

Rachma Prilian Eviningsih [a], Ewa Ari Irwansyah [a], Epyk Sunarno [a,] *, Moh Zaenal Efendi [a], Novie Ayub Windarko [a], Anggara Trisna Nugraha [b, c]

[a] *Electrical Engineering Department, Politeknik Elektronika Negeri Surabaya Jalan Raya ITS Sukolilo Kampus PENS, Surabaya, 60111, Indonesia*

[b] *Department of Bio-Industrial Mechatronics Engineering, National Chung Hsing University Taichung, 402202, Taiwan*

[c] *Associate Degree Department of Marine Electrical Engineering, Shipbuilding Institute of Polytechnic Surabaya Surabaya 60111, Indonesia*

Abstract

Photovoltaic efficiency is frequently compromised by physical obstructions, resulting in partial shading conditions. This non-uniform irradiance condition severely distorts system characteristics by inducing multiple power peaks. This study proposes a novel fractional tent map-chaotic horse herd optimization (FTM-CHHO) algorithm for global maximum power point (GMPP). By integrating fractional-order memory and chaotic maps, FTM-CHHO enhances global search capabilities and prevents entrapment in local maxima. The method was rigorously validated through simulations and hardware experiments using a SEPIC converter. Simulations demonstrated that FTM-CHHO achieved 99.52 % to 100 % tracking accuracy with rapid convergence times of 0.32 to 0.62 s. Furthermore, hardware tests under real-world shading confirmed its robustness, maintaining 95.54 % to 98.26 % accuracy and converging within 10.1 s. FTM-CHHO significantly outperformed perturb and observe (P&O) and standard horse herd optimization (HHO). These findings confirm that FTM-CHHO provides a highly reliable, fast, and efficient solution for maximizing solar energy extraction under complex environmental variability.

Keywords: fractional tent map-chaotic horse herd optimization (FTM-CHHO); photovoltaic systems; partial shading conditions;.

I. Introduction

The escalating global demand for renewable energy has established solar photovoltaic (PV) systems as a fundamental component of modern power generation [1]. However, PV efficiency is inherently sensitive to environmental fluctuations and non-linear electrical characteristics [2]. To maximize energy extraction under varying weather conditions, implementing a robust maximum power point tracking (MPPT) controller is an absolute necessity [3].

A critical operational challenge in PV arrays is the occurrence of partial shading conditions. When bypass diodes are activated during partial shading, the power-voltage (P-V) characteristics distort, producing multiple power peaks. This multi-peak phenomenon demands advanced tracking algorithms to pinpoint the true global maximum power point (GMPP).

* Corresponding Author. epyk@pens.ac.id (E. Sunarno)

https://doi.org/10.55981/j.mev.2026.1423

Received 19 April 2026; revised 8 May 2026; accepted 18 May 2026; available online 7 July 2026; published 31 July 2026

How to Cite: R. P. Eviningsih *et. al.*, "Fractional tent map-chaotic horse herd optimization for global MPPT under partial shading conditions," *Journal of Mechatronics, Electrical Power, and Vehicular Technology*, vol. 17, no. 1, pp. 90-106, July, 2026.

Conventional MPPT techniques, such as perturb and observe (P&O) and incremental conductance (INC), are favored for their simplicity; yet, they frequently fail under partial shading, causing substantial energy yield reductions due to local entrapment [4].

To overcome these conventional limitations, various metaheuristic optimization algorithms have been widely implemented [5]. While methods such as particle swarm optimization (PSO) and genetic algorithms (GA) improve GMPP tracking, they often suffer from slow convergence, high computational complexity, and steady-state oscillations [5]. Consequently, recent research focuses on developing advanced metaheuristics with faster convergence and higher robustness under partial shading [6], including the implementation of bio-inspired methods such as the modified remora optimization [7]. Furthermore, efforts to improve hardware stability and efficiency have led to the utilization of advanced converter topologies and controls, such as synchronous buck converters [8] and Type III compensators [9]. Building upon these advancements, the integration of tracking algorithms with a single-ended primary-inductor converter (SEPIC) has been recognized as a superior approach due to its continuous input current and wide operating range [10][11].

In this context, horse herd optimization (HHO) has emerged as a promising nature-inspired algorithm, offering a balance between exploration and exploitation [12]. In PV applications, HHO demonstrates good GMPP tracking capability with relatively simple modelling [13]. However, under rapidly changing and complex shading conditions, standard HHO remains prone to premature convergence and power oscillations due to its pseudo-random search mechanism [14].

To improve search diversity, chaotic maps have been introduced to replace random variables, leading to the development of chaotic horse herd optimization (CHHO), which enhances global exploration and reduces local entrapment [15]. Nevertheless, conventional chaotic maps still lack a memory mechanism, limiting their ability to achieve high-precision convergence in the exploitation phase.

Alternatively, fractional-order calculus has been widely recognized for its memory and hereditary properties, which can significantly enhance optimization performance [16]. Despite its potential, the integration of fractional-order chaotic dynamics into HHO for MPPT under partial shading has not been fully explored. Therefore, this study proposes a fractional tent map-chaotic horse herd optimization (FTM-CHHO) algorithm, where the incorporation of fractional-order memory into the chaotic mapping mechanism enhances both exploration and exploitation capabilities, enabling faster convergence and more accurate GMPP tracking under complex shading conditions.

The main contributions of this work are: (1) developing the FTM-CHHO algorithm by integrating fractional-order tent map dynamics into the HHO framework; (2) evaluating its tracking performance under various partial shading scenarios; and (3) validating its effectiveness through both simulation and experimental implementation.

II. Materials and Methods

A. The design of the MPPT system

The proposed MPPT system is systematically designed to continuously extract the maximum available power from the PV array, particularly when subjected to complex partial shading conditions. As comprehensively illustrated in Figure 1, the overall architecture of the system consists of several integrated components: a PV array, a DC-DC single-ended primary-inductor converter (SEPIC), an MPPT controller unit, a pulse width modulation (PWM) generator, and a resistive load. The SEPIC topology is specifically chosen as the power electronic interface

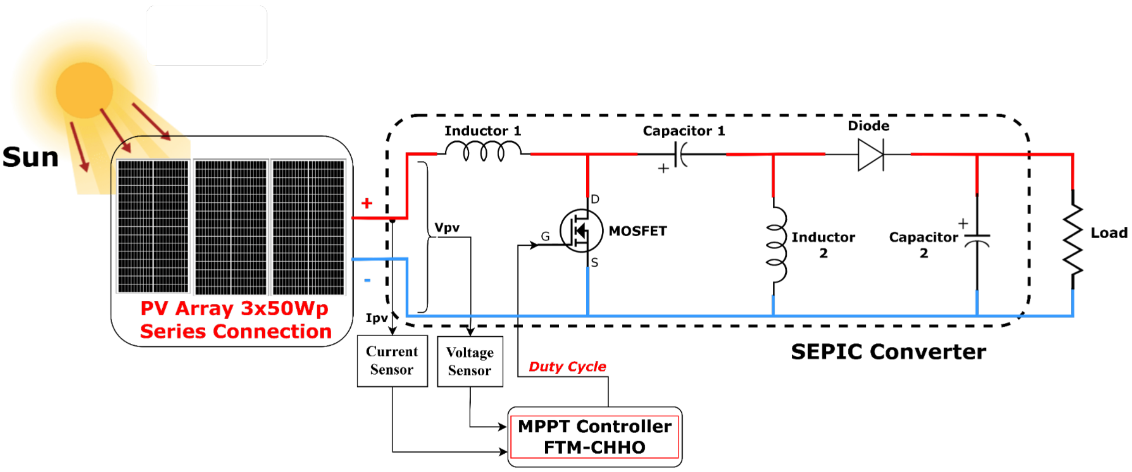

Figure 1. The block diagram of the MPPT system.

between the PV source and the load due to its continuous input current characteristic and its capability to step up or step down the voltage without reversing its polarity.

During the dynamic operation, the instantaneous voltage (V_{PV}) and current (I_{PV}) generated by the solar array are continuously measured using precision sensors and fed directly into the MPPT controller. The controller, which is driven by the proposed FTM-CHHO algorithm, processes these input signals to dynamically compute and update the optimal duty cycle (d). Subsequently, the PWM block translates this optimal duty cycle into high-frequency switching signals directed to the gate of the SEPIC converter's MOSFET. This closed-loop mechanism continuously adjusts the operating point of the converter, thereby forcing the PV system to operate precisely at the true GMPP.

B. Photovoltaic system

PV systems generate electricity by converting solar irradiance into direct current (DC) through the photovoltaic effect. Due to the inherent physics of semiconductor materials, the output performance of a PV module is highly non-linear and significantly depends on environmental factors, particularly solar irradiance and temperature [17]. Therefore, an accurate mathematical model is essential to simulate and analyze the PV system's behavior under various conditions before deploying the MPPT algorithm.

To mathematically analyze this non-linear behavior, a practical single-diode equivalent circuit model is employed. As comprehensively illustrated in Figure 2, this model accurately represents the physics of a practical solar cell. It comprises a photocurrent source (I_{ph}) that depends on irradiance, a parallel diode (D) representing the p-n junction characteristics, a parallel (shunt) resistance (R_{sh}) accounting for leakage currents, and a series resistance (R_s) representing internal losses at the contacts and semiconductor materials.

By applying Kirchhoff's current law to the nodes in Figure 2, the fundamental equation that describes the current-voltage (I-V) characteristics of the single-diode model is derived and expressed by the characteristic transcendent equation (1).

$$\mathrm{I} = \mathrm{I_{ph}} - \mathrm{I_0}\left[\exp\left(\frac{\mathrm{q(V+IR_s)}}{\mathrm{nkT}}\right) - 1\right] - \frac{\mathrm{V+IR_s}}{\mathrm{R_{sh}}} \tag{1}$$

It is critical to observe that the generated photocurrent I_{ph} is not constant; it varies linearly with the actual solar irradiance (G) and is slightly influenced by the actual cell temperature (T). This dynamic dependency is mathematically defined in equation (2).

$$\mathrm{I_{ph}} = \left[\mathrm{I_{sc,ref}} + \alpha_\mathrm{i}(\mathrm{T} - \mathrm{T_{ref}})\right]\frac{\mathrm{G}}{\mathrm{G_{ref}}} \tag{2}$$

where I is the output current (A) and V is the output voltage (V). I_{ph} represents the dynamic generated photocurrent (A), and I_0 is the diode reverse saturation current (A). The constant q denotes the electron charge (1.602×10^{-19} C), k is the Boltzmann constant (1.381×10^{-23} J/K), and n is the diode ideality factor. R_s and R_{sh} represent the series and shunt resistances (Ω), respectively. In equation (2), $I_{sc,ref}$ is the short-circuit current at reference standard test conditions (STC), α_i is the temperature coefficient of the short-circuit current (A/K), G and G_{ref} are the actual and reference solar irradiance (1000 W/m²), and T and T_{ref} are the actual and reference cell temperatures (298.15 K).

In this study, a practical 50 Wp PV module is utilized to evaluate the proposed MPPT performance. The detailed electrical specifications of this specific PV module under standard test conditions (STC) are summarized and provided in Table 1.

C. Partial shading condition

In outdoor environments, PV arrays frequently experience non-uniform irradiance, known as partial shading conditions, caused by obstacles like passing clouds or trees [18]. Under partial shading, shaded cells generate lower photocurrents and act as passive loads, risking severe thermal damage through the hot-spot

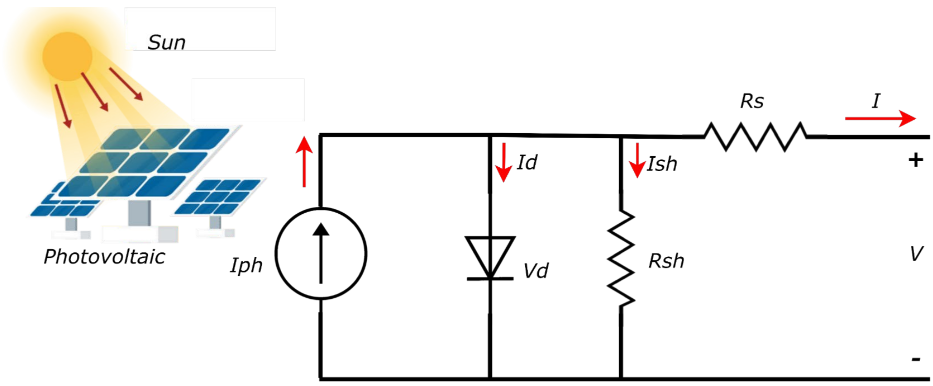

Figure 2. Electrical equivalent circuit of a solar cell.

phenomenon [19]. To prevent this destructive effect, bypass diodes are connected in anti-parallel across the modules to provide alternative current paths [19]. However, while this hardware intervention ensures thermal protection, it fundamentally alters the array's electrical characteristics, creating a staircase-like current-voltage (I-V) profile and inducing multiple peak points on the power-voltage (P-V) curve [20].

As comprehensively illustrated in Figure 3, the system's P-V characteristics behave distinctly based on the shading patterns. While uniform irradiance, designated as Pattern 1, yields a single convex peak, non-uniform profiles designated as Patterns 2–5 exhibit a complex multi-peak phenomenon characterized by several local maximum power points (LMPPs) and exactly one true global maximum power point (GMPP) [20]. This multi-peak nature poses a severe tracking challenge, as conventional MPPT controllers relying on basic gradient-climbing logic inevitably trapped at the first encountered LMPP, leading to substantial energy losses [18]. Consequently, implementing an advanced, highly explorative metaheuristic algorithm is strictly required to dynamically bypass these local traps and successfully pinpoint the true GMPP under any partial shading scenario.

D. DC-DC SEPIC converter

To optimally transfer the maximum available power from the PV array to the load, a DC-DC converter acts as the crucial impedance-matching interface. In this proposed architecture, SEPIC, as comprehensively illustrated in Figure 4, is systematically selected over conventional topologies such as Buck, Boost, or standard Buck-Boost converters. The primary justification for this selection lies in the SEPIC's inherent capability to step-up or step-down the input voltage without reversing the output voltage polarity [21].

More importantly for MPPT applications, the SEPIC topology features an inductor (L_1) at its input terminal. This configuration guarantees a strictly continuous input current, which fundamentally minimizes high-frequency harmonic ripples drawn from the PV array [22]. A continuous and ripple-free input current is highly critical, as it allows the proposed FTM-CHHO algorithm to sense the PV voltage and current accurately, thereby preventing the agents from diverging during the sensitive exploitation phase [10].

The converter is meticulously designed to operate in the continuous conduction mode (CCM) to ensure a steady power flow. The dynamic relationship between the input voltage (V_{in}) generated by the PV array and

Table 1.
Electrical specifications of the utilized 50 Wp PV module.

Parameter	Value
Maximum power (P_{max})	50 W
Voltage at maximum power point (V_{mp})	18.0 V
Current at maximum power point (I_{mp})	2.78 A
Open-circuit voltage (V_{oc})	21.4 V
Short-circuit current (I_{sc})	2.95 A
Temperature coefficient of I_{sc} (α_i)	0.065 %/°C
Temperature coefficient of V_{oc}	-0.40 %/°C
Number of cells connected in series (N_s)	32

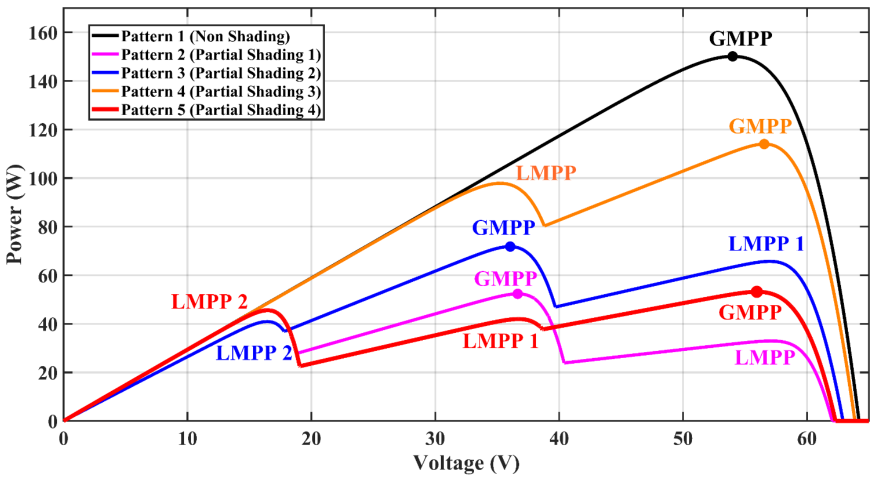

Figure 3. P-V Characteristics under various shading conditions.

the required output voltage (V_{out}) across the load is dictated by the duty cycle (D) of the active MOSFET switch (SW). Ignoring the minor voltage drops across the switching components, the fundamental voltage transfer ratio is mathematically expressed in equation (3).

$$V_{out} = V_{in}\left(\frac{D}{1-D}\right) \tag{3}$$

Consequently, to maintain the system at the GMPP, the MPPT controller continuously adjusts the ideal duty cycle according to equation (4).

$$D = \frac{V_{out}}{V_{in}+V_{out}} \tag{4}$$

To physically construct the proposed SEPIC hardware prototype, the reactive energy-storage components must be critically sized based on the predefined switching frequency (f_s) and the acceptable ripple tolerances. The input inductor (L_1) and the output inductor (L_2) are strictly calculated to limit the peak-to-peak current ripples (ΔI_{L1} and ΔI_{L2}) within a specific percentage of the continuous current. The minimum required inductances are determined using equation (5) and equation (6) [23]:

$$L_1 = \frac{V_{in}\cdot D}{\Delta I_{L1}\cdot f_s} \tag{5}$$

$$L_2 = \frac{V_{in}\cdot D}{\Delta I_{L2}\cdot f_s} \tag{6}$$

Furthermore, the coupling capacitor (C_1), which is responsible for transferring energy from the input to the output stage, and the output filter capacitor (C_2), which stabilizes the voltage across the load, are calculated to strictly restrict the voltage ripples (ΔV_{C1} and ΔV_{out}). Their minimum required capacitance values are mathematically synthesized in equation (7) and equation (8) [23]:

$$C_1 = \frac{I_{out}\cdot D}{\Delta V_{C1}\cdot f_s} \tag{7}$$

$$C_2 = \frac{I_{out}\cdot D}{\Delta V_{out}\cdot f_s} \tag{8}$$

By properly sizing these parameters, the SEPIC converter is fully optimized to execute the rapid and aggressive duty cycle variations commanded by the FTM-CHHO controller during extreme partial shading transitions. Based on the previously discussed mathematical design equations and the specific electrical characteristics of the utilized PV module, the optimal parameters for the proposed SEPIC converter have been rigorously calculated. The detailed electrical specifications and the selected component values employed for both the simulation study and the experimental hardware prototype are systematically summarized in Table 2.

E. Horse herd optimization (HHO)

The HHO is an advanced population-based metaheuristic algorithm fundamentally inspired by the complex social, herding, and hierarchical behaviors of wild horses in nature [24]. To mathematically translate these natural behaviors into a robust optimization search process, the algorithm systematically divides the total population of horses (agents) into four distinct age groups with predefined proportions: δ horses (foals, 0–5 years old) representing 40 %, γ horses (young, 5–10

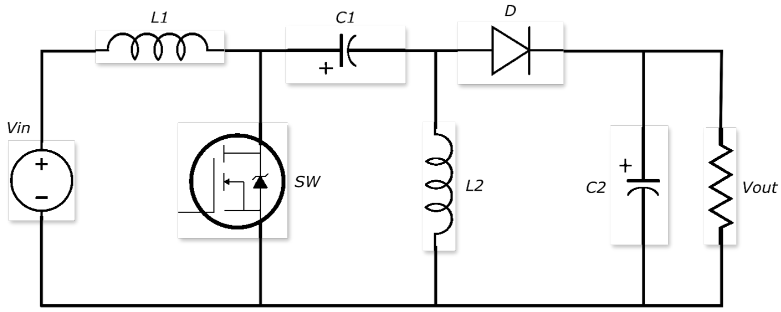

Figure 4. SEPIC converter circuit.

Table 2.
Electrical specifications and component parameters of the proposed SEPIC converter.

Parameter	Value
Switching frequency (f_s)	40 kHz
Input inductor (L_1)	512 µH
Output inductor (L_2)	512 µH
Coupling capacitor (C_1)	586 µF
Output capacitor (C_2)	586 µF
Load resistance (R_L)	9 Ω

years old) representing 30 %, β horses (adults, 10–15 years old) representing 20 %, and α horses (elderly, >15 years old) representing 10 % of the total herd [12][24].

The movement trajectory and position updating of each horse during the optimization iterations are strictly governed by a combination of six primary behavioral operators: Grazing (G), hierarchy (H), sociability (S), imitation (I), defense mechanism (D), and roaming (R) [13]. The unique combination of these behavioral matrices dictates the velocity (V) of the horses depending on their specific age group. The mathematical formulation for the velocity update of each age category is systematically expressed in equation (9) through equation (12) [24].

$$V_m^{Iter,\delta} = G_m^{Iter,\delta} + R_m^{Iter,\delta} \quad (9)$$

$$V_m^{Iter,\gamma} = G_m^{Iter,\gamma} + H_m^{Iter,\gamma} + S_m^{Iter,\gamma} + I_m^{Iter,\gamma} + D_m^{Iter,\gamma} + R_m^{Iter,\gamma} \quad (10)$$

$$V_m^{Iter,\beta} = G_m^{Iter,\beta} + H_m^{Iter,\beta} + S_m^{Iter,\beta} + D_m^{Iter,\beta} \quad (11)$$

$$V_m^{Iter,\alpha} = G_m^{Iter,\alpha} + D_m^{Iter,\alpha} \quad (12)$$

where $V_m^{Iter,AGE}$ denotes the computational velocity vector of the m-th horse at the current iteration ($Iter$) for a specific age group. Following the calculation of the velocity based on the designated behaviors, the new position of each horse in the search space—which practically corresponds to the operating duty cycle in the PV MPPT application—is updated using equation (13) [13].

$$X_m^{Iter,AGE} = X_m^{Iter-1,AGE} + V_m^{Iter,AGE} \quad (13)$$

where $X_m^{Iter,AGE}$ and $X_m^{Iter-1,AGE}$ represent the current and previous positions (duty cycles) of the m-th horse, respectively. This distinct age-based mathematical mechanism allows the standard HHO to maintain a robust balance between global exploration (primarily driven by the highly active young δ and γ horses) and local exploitation (executed by the mature β and α horses) to track the GMPP [12].

To rigorously construct the velocity vectors previously defined in equation (9) to equation (12), the HHO algorithm translates the natural instincts of wild horses into six distinct mathematical operators [24]. In the context of MPPT, the position of each horse fundamentally represents the operating duty cycle (X_m). These behavioral operators are dynamically calculated as follows [13][24]:

1. Grazing (G)

This operator mimics the continuous foraging behavior of horses. It enables a gradual, localized search around the current position to finely tune the duty cycle and minimize power oscillations is expressed in equation (14).

$$G_m^{Iter,AGE} = g_m^{Iter} \times (l_w + \xi \times u_p) \times X_m^{Iter-1} \quad (14)$$

where g_m^{Iter} is the grazing weight that decreases linearly per iteration, ξ is a random number generated between 0 and 1, while l_w and u_p define the lower and upper bounds of the grazing space.

2. Hierarchy (H)

Reflecting the instinct of a herd to follow the strongest leader, this operator exerts an attractive force that pulls the agents toward the best-performing duty cycle (X_{best}) discovered so far is expressed in equation (15).

$$H_m^{Iter,AGE} = h_m^{Iter} \times (X_{best}^{Iter-1} - X_m^{Iter-1}) \quad (15)$$

where h_m^{Iter} represents the velocity coefficient of the hierarchical law.

3. Sociability (S)

To ensure herd survival, horses tend to move toward the center of the group. This prevents the duty cycle from scattering too far from potentially optimal power regions according to equation (16).

$$S_m^{Iter,AGE} = s_m^{Iter} \times \left(\frac{1}{N}\sum_{j=1}^{N} X_j^{Iter-1} - X_m^{Iter-1}\right) \quad (16)$$

where N is the total population of the horse herd.

4. Imitation (I)

Young horses frequently copy the habits of the most successful individuals. Mathematically, it guides the agents toward the average position of the top pN horses (the best p % of the population that produces the highest PV power) is expressed in equation (17).

$$I_m^{Iter,AGE} = i_m^{Iter} \times \left(\frac{1}{pN}\sum_{j=1}^{pN} \hat{X}_j^{Iter-1} - X_m^{Iter-1}\right) \quad (17)$$

where $\hat{X}_j$ denotes the positions of the superior horses.

5. Defense mechanism (D)

In nature, horses instinctively flee from hazardous environments. In the MPPT landscape, this acts as a repulsive force that actively pushes the agents away from suboptimal or low-yield LMPPs, represented by the worst qN horses is expressed in equation (18).

$$D_m^{Iter,AGE} = -d_m^{Iter} \times \left(\frac{1}{qN}\sum_{j=1}^{qN} \check{X}_j^{Iter-1} - X_m^{Iter-1}\right) \quad (18)$$

where $\check{X}_j$ represents the worst performing duty cycles. The negative sign inherently provides the escape velocity vector.

6. Roaming (R)

This operator simulates the curious, random wandering of young horses seeking new pastures, which fundamentally enhances the global exploration capability to rapidly detect the true GMPP under complex shading.

$$R_m^{Iter,AGE} = r_m^{Iter} \times \xi \times X_m^{Iter-1} \quad (19)$$

For all the aforementioned operators, the adaptive behavioral weights (g_m, h_m, s_m, i_m, d_m, and r_m) are systematically reduced at each iteration using specific decay factors (ω). This reduction mechanism is highly critical as it guarantees the swift convergence of the MPPT controller once the GMPP is successfully pinpointed [24].

F. The proposed FTM-CHHO

1. The fundamental of chaotic maps

Standard HHO relies on pseudo-random number generators for population initialization and behavioral execution. However, this randomization frequently produces non-uniform search space distributions and low population diversity, inherently increasing the risk of entrapment at LMPPs under complex shading [14][15]. To mitigate this, deterministic chaotic maps—characterized by unpredictable and ergodic properties—are introduced to replace random variables, thereby ensuring a highly comprehensive exploration of the search space [14][16]. Recent literature corroborates that utilizing such chaotic trajectories instead of traditional randomness significantly amplifies global exploration capabilities and effectively prevents premature convergence at local optima [25].

2. Standard chaotic tent map (CTM)

Among various chaotic mapping functions (such as logistic, sine, or gauss maps), the tent map is specifically selected in this study due to its superior uniform distribution and higher ergodicity compared to other maps [14][16]. Mathematically, a standard one-dimensional chaotic tent map (CTM) is defined by the following piecewise linear equation (20).

$$x_{k+1} = \begin{cases} \frac{x_k}{\mu}, & 0 \le x_k < \mu \\ \frac{1-x_k}{1-\mu}, & \mu \le x_k \le 1 \end{cases} \quad (20)$$

where x_k represents the chaotic sequence value at iteration k, and μ is the control parameter (typically set to 0.5 to maximize chaos in the standard integer-order map; note that this differs from the fractional chaotic control parameter μ = 1.9 used in the proposed FTM implementation, which follows the formulation introduced in [15]. As emphasized in previous research [14][16], the tent map provides a better "spread" of agents across the P-V curve, which is fundamental for detecting the true global maximum power point (GMPP) during the early stages of optimization. However, standard CTM remains an integer-order system where each state depends only on its immediate predecessor, thereby lacking a dynamic memory of its historical trajectory.

3. FTM and its memory effect

To overcome the "memoryless" nature of standard maps, the core novelty of the proposed FTM-CHHO lies in the integration of fractional-order calculus. Unlike standard integer-order derivatives, a fractional-order map introduces a robust "hereditary property" [16]. This allows the chaotic trajectory to inherently retain and process information from all previous states, creating a smoother and more intelligent convergence path. Based on the Grünwald-Letnikov (GL) fractional calculus definition, the proposed FTM at iteration T is rigorously formulated as equation (21).

$$x_{T+1} = x_0 + \frac{1}{\Gamma(\alpha)} \sum_{j=1}^{T} \frac{\Gamma(T-j+\alpha)}{\Gamma(T-j+1)} \min\big((\mu-1)x_{j-1}, \mu - (\mu+1)x_{j-1}\big) \quad (21)$$

In this formulation, x_{T+1} is the newly generated fractional chaotic variable, x_0 is the initial sequence value, α denotes the specific fractional order ($0 < \alpha \le 1$), and μ is the chaotic bifurcation parameter. The Gamma function (Γ) mathematically facilitates the computation of the fractional-order derivative [16]. The integration of such fractional calculus concepts introduces a robust long-term memory mechanism that adaptively balances the exploration and exploitation phases throughout the optimization process [26]. By capitalizing on these mathematical phenomena alongside chaotic mapping, advanced metaheuristic approaches are proven to achieve smoother and more reliable convergence trajectories in highly complex energy harvesting problems [27].

4. The integration into HHO (FTM-CHHO)

The systematic execution of the proposed FTM-CHHO algorithm, comprehensively illustrated in Figure 5, begins by initializing fundamental parameters such as maximum iterations, horse agents (N), and specific FTM parameters (α and q). Replacing the standard pseudo-random generator, the FTM creates a highly uniform chaotic population mapped within predefined duty cycle boundaries (D_{min} to D_{max}). This strategic P-V curve coverage significantly accelerates GMPP detection [14][15]. During initial tracking, the SEPIC converter is driven by these chaotic duty

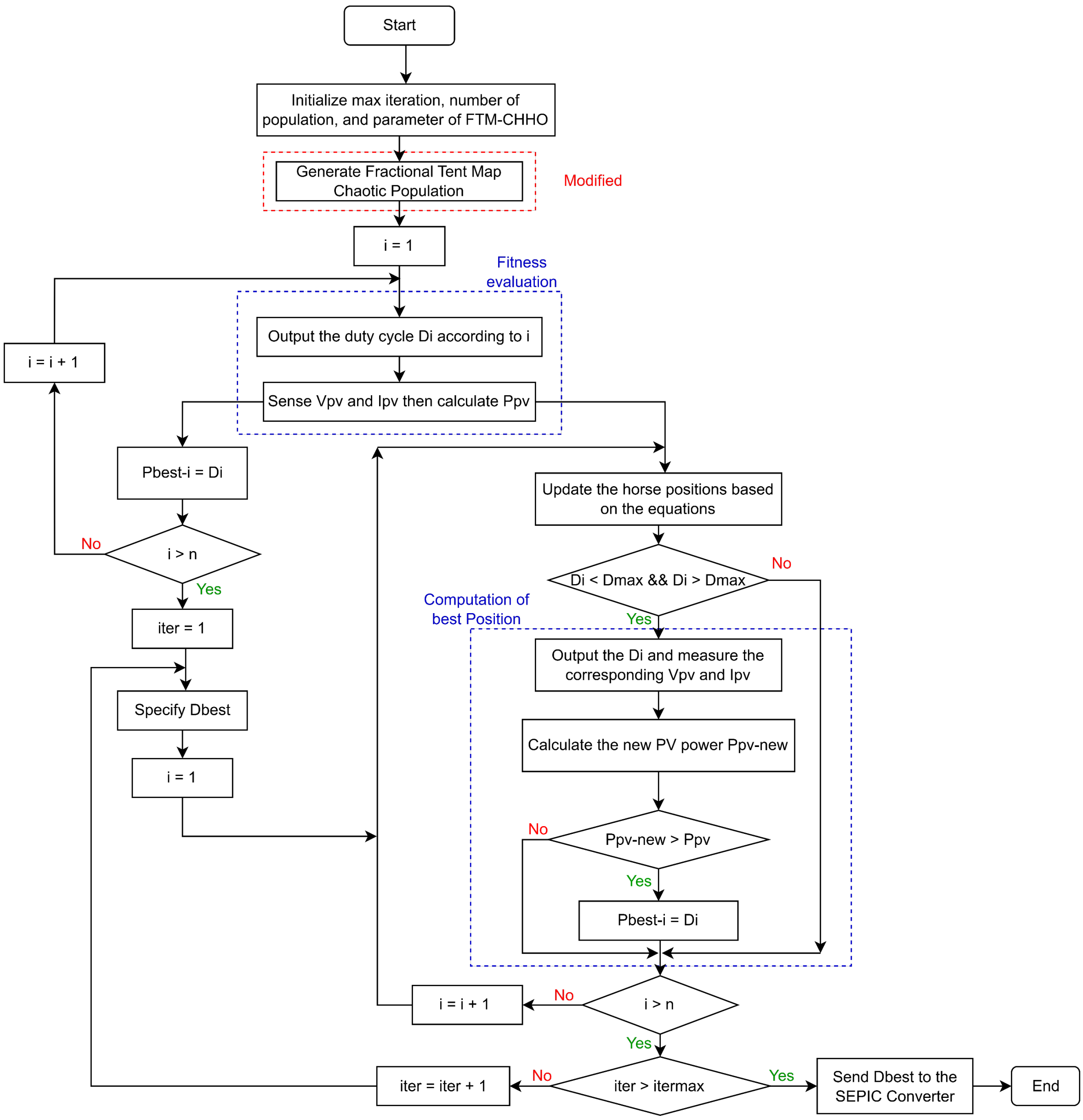

Figure 5. The flowchart of FTM –CHHO for MPPT.

cycles (D_i), while sensors measure PV voltage (V_{pv}) and current (I_{pv}) to calculate instantaneous power (P_{pv}) and record the initial best position (D_{best}). In the main optimization loop, horses update their positions via age-group equations (equation (9) to equation (13)), where the fractional chaotic variable (C_i) dynamically replaces the standard random parameter (r) [15]. This endows the algorithm with aggressive global exploration to quickly bypass multiple LMPPs [14][15], while ensuring new duty cycles remain within safe operating limits. Finally, if the newly measured PV power exceeds the previous value, the algorithm updates D_{best}. This fractional memory-driven exploitation ensures precise settling at the GMPP with virtually zero steady-state oscillations [14][16]. Once maximum iterations are reached, the global optimum duty cycle (D_{GMPP}) is continuously transmitted to extract maximum energy. The monumental advantage of combining fractional-order memory with chaotic ergodicity to completely eliminate power ripples and accelerate convergence has been extensively validated by recent advanced PV optimization studies [28][29].

III. Results and Discussions

A. Simulation results

To thoroughly evaluate the dynamic tracking performance and robustness of the proposed FTM-CHHO algorithm, a comprehensive simulation study was strictly executed. As comprehensively illustrated in Figure 6, the complete simulation architecture was meticulously constructed by integrating several vital subsystems. These subsystems encompass a 150 Wp PV array formed by three series-connected 50 Wp modules equipped with parallel bypass diodes, a high-frequency DC-DC SEPIC converter, a resistive load, precision voltage and current measurement blocks, and the central MPPT controller embedding the proposed FTM-CHHO algorithm.

The MPPT performance of the FTM-CHHO was systematically benchmarked against two well-established algorithms: the conventional P&O and the standard HHO. The specific parameter settings utilized during the simulation phase are comprehensively summarized in Table 3.

During the simulation testing, the population size was uniformly set to four agents across all evaluated algorithms to ensure a fair and consistent computational assessment. To ensure a fair comparison, all evaluated algorithms were implemented under identical operating bounds, converter specifications, irradiance scenarios, and population sizes. Meanwhile, several algorithm-specific coefficients, including behavioral weights and chaotic control parameters, were retained according to the recommended stable settings reported in their original formulations to preserve convergence stability and avoid abnormal tracking behavior during GMPP searching. The tracking efficacy of the proposed FTM-CHHO algorithm was rigorously validated under two primary environmental states: uniform irradiance (without shading) and partial shading conditions. Table 4 details

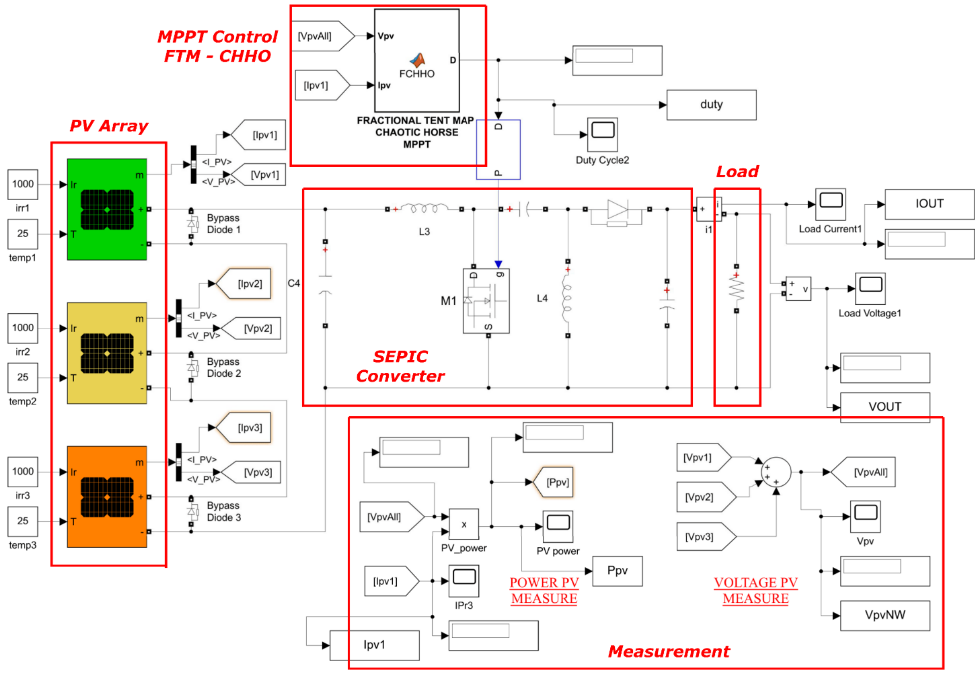

Figure 6. Simulation model of the proposed MPPT system.

Table 3.
Control parameters of the implemented MPPT algorithms.

Algorithm	Parameter	Value
Perturb and observe (P&O)	Initial duty cycle (D_{init})	0.1
	Perturbation step size (ΔD)	10^{-4}
	Operating bounds	[0.1, 0.9]
Horse herd optimization (HHO)	Population size (N)	4
	Initial duty cycles	[0.55, 0.2, 0.85, 0.4]
	Base behavioral weight (xx)	0.6
	Inertia weight (w)	0.8
	Operating bounds	[0.1, 0.9]
Fractional tent map chaotic horse herd optimization (FTM-CHHO)	Population size (N)	4
	Chaotic map type	Fractional tent map
	Chaotic initial value (x_0)	0.7
	Chaotic parameter (μ)	1.9
	Fractional derivative order (α)	0.6
	Base behavioral weight (xx)	0.8
	Operating bounds	[0.1, 0.9]

the specific irradiance configurations applied to the three series-connected PV modules, which were precisely adjusted to emulate real-world shading profiles.

Table 4 presents the five distinct irradiance configurations designed for the simulation, alongside their respective GMPP values. The corresponding power-voltage (P-V) characteristics for each configuration are depicted in Figure 7. Pattern 1 represents a uniform irradiance condition that produces a single peak on the P-V curve. In contrast, patterns 2–5 correspond to partial shading conditions that generate multiple LMPPs and a single GMPP due to irradiance mismatch among PV modules and bypass diode activation. The detailed irradiance configurations and GMPP values are summarized in Table 4. These multi-peak characteristics create a complex non-linear search space, making them suitable for evaluating the tracking capability of the proposed MPPT algorithms.

Figure 8 illustrates the duty cycle (a) and power response (b) for Pattern 1 under uniform irradiance. Targeting a 145.52 W GMPP, the proposed FTM-CHHO achieves flawless 100 % accuracy in just 0.43 s. Conversely, P&O also reaches 100.00 % but required 0.57 s, whereas standard HHO achieves only 99.77 % accuracy, converging at 145.18 W in 0.54 s.

Figure 9 illustrates the dynamic tracking performances under various partial shading conditions. Across all tested patterns, the proposed FTM-CHHO

Table 4.
Simulation test patterns under various irradiance configurations.

Pattern	PV 1	PV 2	PV 3	GMPP
Pattern 1	1000 W/m²	1000 W/m²	1000 W/m²	145.52 W
Pattern 2	520 W/m²	800 W/m²	1000 W/m²	85.31 W
Pattern 3	1000 W/m²	333 W/m²	700 W/m²	72.50 W
Pattern 4	800 W/m²	200 W/m²	300 W/m²	36.28 W
Pattern 5	770 W/m²	770 W/m²	300 W/m²	74.89 W

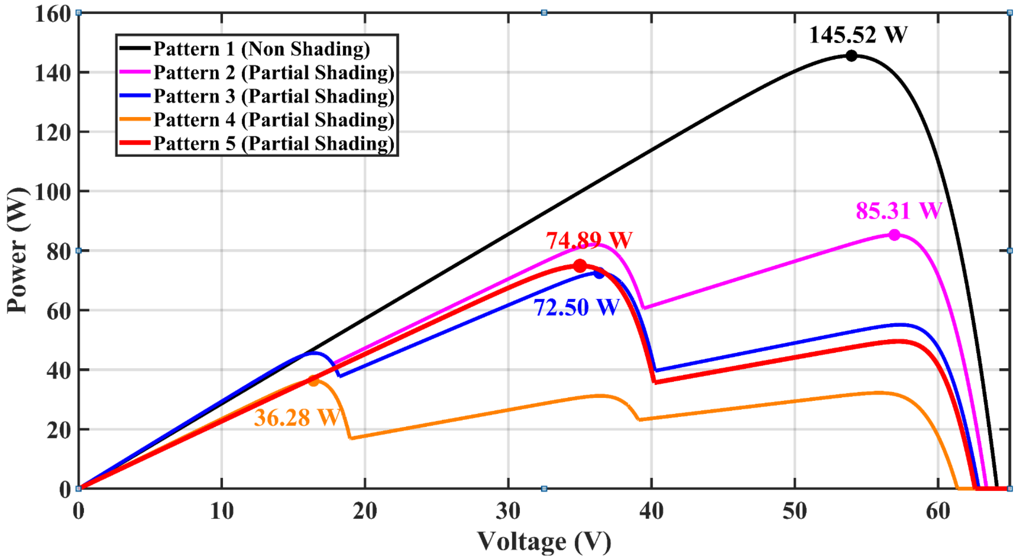

Figure 7. Simulated P-V characteristics of the PV array.

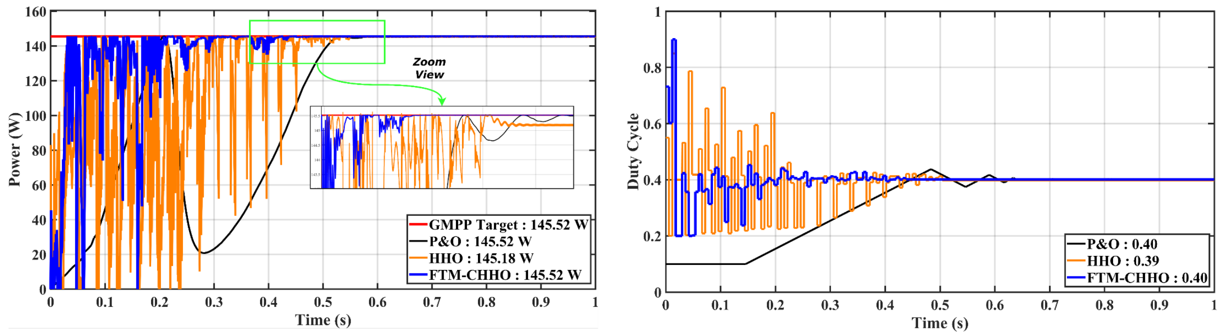

(a) (b)

Figure 8. Simulation results under Pattern 1. (a) power response; (b) duty cycle.

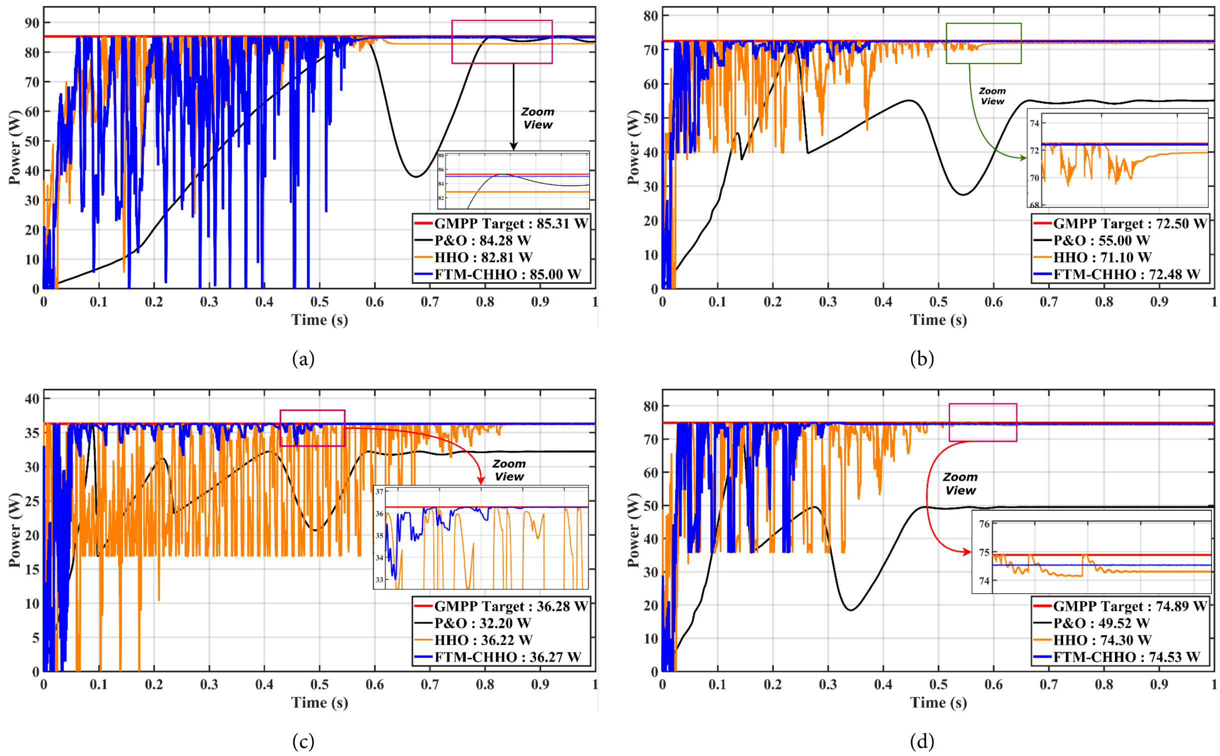

Figure 9. Simulation tracking results under partial shading conditions. (a) pattern 2; (b) pattern 3; (c) pattern 4; (d) pattern 5.

Table 5.
Quantitative tracking performance comparison of the evaluated MPPT algorithms.

Pattern	GMPP	Algorithm	Power MPPT	Accuracy	Tracking time
Pattern 1	145.52 W	P&O	145.52 W	100.00 %	0.57 s
		HHO	145.18 W	99.77 %	0.54 s
		FTM-CHHO	145.52 W	100.00 %	0.43 s
Pattern 2	85.31 W	P&O	84.28 W	98.79 %	0.79 s
		HHO	82.81 W	97.07 %	0.64 s
		FTM-CHHO	85.00 W	99.64 %	0.58 s
Pattern 3	72.50 W	P&O	55.00 W	75.86 %	0.86 s
		HHO	71.10 W	98.07 %	0.58 s
		FTM-CHHO	72.48 W	99.97 %	0.37 s
Pattern 4	36.28 W	P&O	32.20 W	88.75 %	0.77 s
		HHO	36.22 W	99.83 %	0.84 s
		FTM-CHHO	36.27 W	99.97 %	0.51 s
Pattern 5	74.89 W	P&O	49.52 W	66.12 %	0.61 s
		HHO	74.30 W	99.21 %	0.65 s
		FTM-CHHO	74.53 W	99.52 %	0.32 s

consistently achieves high tracking accuracy with faster convergence than the standard HHO and conventional P&O methods. The detailed quantitative results are summarized in Table 5. Compared to HHO, FTM-CHHO demonstrates shorter convergence times and more stable tracking behavior, while the P&O algorithm frequently experiences local entrapment under complex shading patterns, resulting in lower power extraction efficiency. These results indicate that the integration of fractional memory and chaotic exploration improves GMPP tracking performance under partial shading conditions. A comprehensive quantitative comparison detailing the theoretical GMPP, extracted power, tracking accuracy, and convergence time for all evaluated algorithms is systematically summarized in Table 5.

To further evaluate the adaptability and robustness of the proposed FTM-CHHO under rapidly changing weather conditions, a dynamic irradiance simulation was conducted. As illustrated in Figure 10, the irradiance levels were intentionally varied over time to simulate sudden and severe shading transitions across the PV array.

The tracking results demonstrate that FTM-CHHO provides fast and stable dynamic responses under changing irradiance conditions. Following each environmental transition, the algorithm successfully re-tracked the GMPP with minimal steady-state oscillations and shorter convergence times than the compared methods, indicating reliable performance under dynamic operating conditions.

B. Experimental hardware results

Figure 11 shows the hardware implementation of the proposed MPPT system, consisting of series-connected PV modules, a SEPIC converter, sensing circuits, a microcontroller, and a resistive load. Experimental tests were conducted under real outdoor conditions to evaluate the tracking performance of the P&O, HHO, and FTM-CHHO algorithms under identical operating conditions. System data were recorded to analyze tracking speed, power extraction, and steady-state stability.

Furthermore, the empirical Power-Voltage (P-V) characteristics captured during the baseline measurement are illustrated in Figure 12, establishing the absolute GMPP reference for the subsequent hardware validations.

Figure 13 presents the experimental tracking performance under the uniform irradiance condition (Pattern 1), including the power response and duty cycle characteristics. The detailed quantitative results are summarized in Table 6. Compared with P&O and standard HHO, the proposed FTM-CHHO achieves faster convergence and more stable steady-state tracking with reduced oscillations.

Figure 14(a) presents the hardware tracking response during the Pattern 2 scenario. Targeting a baseline GMPP of 85.64 W, the introduced FTM-CHHO extracted 84.15 W, which corresponds to an accuracy of 98.26 %, in just 8.7 s. Conversely, the standard HHO consumes 21.1 s to reach 81.54 W, translating to a 95.21 % accuracy. Meanwhile, the conventional P&O algorithm exhibits lower tracking performance, securing 78.34 W, or a 91.48 % precision, after 22.4 s. Furthermore, the dynamic power extraction behaviors during Pattern 3, Pattern 4, and Pattern 5 are explicitly depicted in the grouped experimental results shown in Figure 14(b),

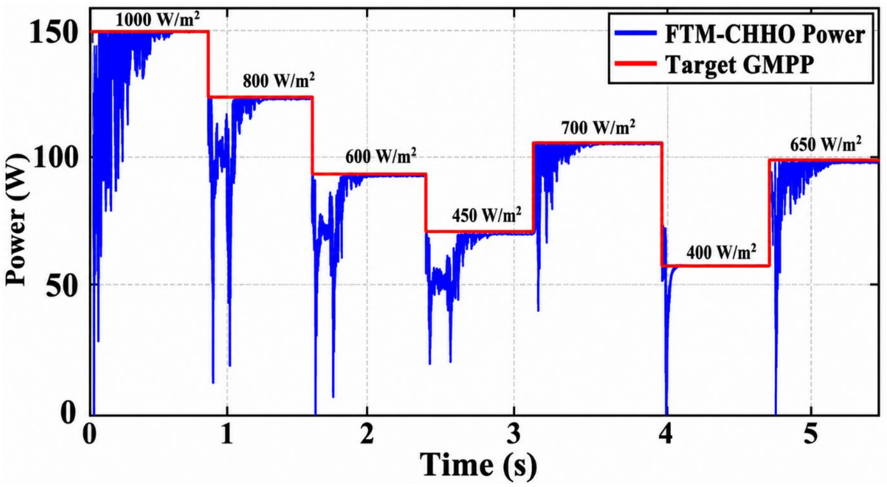

Figure 10. Dynamic tracking performance under varying irradiance conditions.

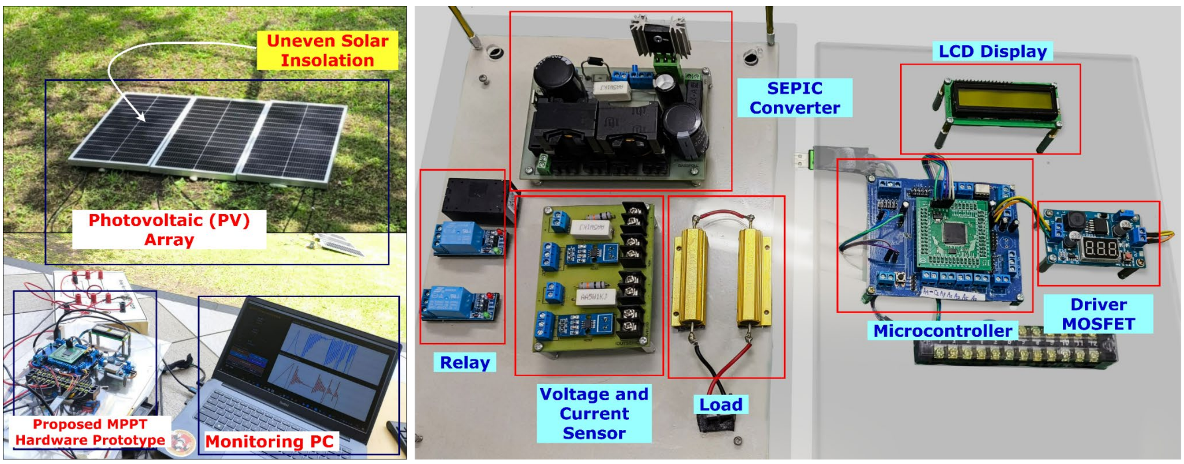

Figure 11. The experimental hardware setup of the proposed MPPT system.

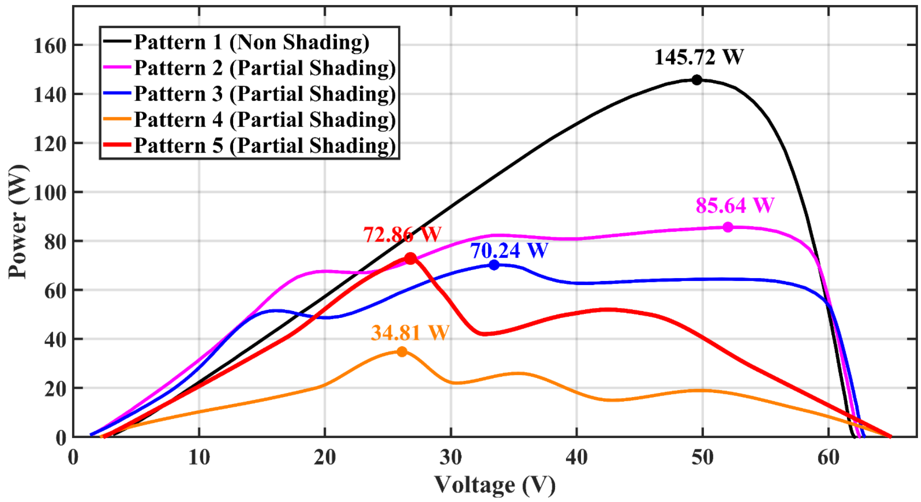

Figure 12. The experimental P-V characteristic curve.

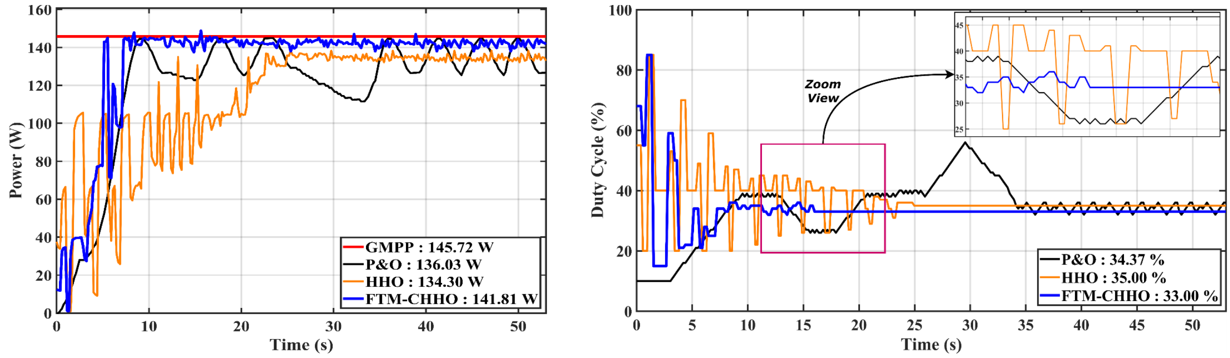

(a) (b)

Figure 13. Experimental results under Pattern 1: (a) power extraction; (b) duty cycle response.

Table 6.
Experimental test results data.

Pattern	GMPP	Algorithm	Power MPPT	Accuracy	Tracking time
Pattern 1	145.72 W	P&O	136.03 W	93.35 %	35.2 s
		HHO	134.30 W	92.16 %	24.9 s
		FTM-CHHO	141.81 W	97.32 %	7.8 s
Pattern 2	85.64 W	P&O	78.34 W	91.48 %	22.4 s
		HHO	81.54 W	95.21 %	21.1 s
		FTM-CHHO	84.15 W	98.26 %	8.7 s
Pattern 3	70.24 W	P&O	58.26 W	82.94 %	19.8 s
		HHO	65.51 W	93.27 %	25.9 s
		FTM-CHHO	67.11 W	95.54 %	9.8 s
Pattern 4	34.81 W	P&O	26.14 W	75.09 %	25.1 s
		HHO	30.95 W	88.91 %	23.6 s
		FTM-CHHO	34.18 W	98.19 %	9.8 s
Pattern 5	72.86 W	P&O	60.28 W	82.73 %	18.6 s
		HHO	63.42 W	87.04 %	27.1 s
		FTM-CHHO	70.07 W	96.17 %	10.1 s

Figure 14(c), and Figure 14(d). Across these complex scenarios, the FTM-CHHO consistently exhibits stable tracking performance.

The detailed quantitative results are summarized in Table 6. The empirical trends indicate that FTM-CHHO consistently maintains tracking accuracies above 95 % across all tested complex scenarios. While standard HHO and P&O experience tracking delays and local entrapment dropping efficiencies to as low as 87.04 % and 75.09 % respectively, the proposed method sustains a stable and rapid global search. The marginal steady-state power deviation observed in FTM-CHHO is primarily attributed to physical switching losses within the SEPIC converter during the chaotic exploration phase, rather than algorithmic stagnation. The improved tracking behavior primarily originates from the integration of fractional-order memory with chaotic exploration. The fractional memory mechanism enables smoother exploitation near the GMPP region, while the Tent Map distribution improves population diversity during the global search process. Consequently, the proposed method reduces premature convergence and stabilizes the tracking trajectory under rapidly changing irradiance conditions.

As quantitatively summarized in Table 6, these empirical outcomes confirm the effectiveness of the proposed controller. By integrating fractional-order memory and chaotic maps, FTM-CHHO achieved real-world tracking accuracies between 95.54 % and 98.26 % with faster convergence performance to under 10.1 s, demonstrating improved tracking performance compared to the conventional methods.

To conclusively validate the real-time adaptability of the proposed system, a dynamic hardware test under continuously varying irradiance was conducted, as illustrated in Figure 15. The experimental results demonstrate that the FTM-CHHO algorithm detects environmental fluctuations and re-establishes the new GMPP with minimal power loss. This rapid dynamic

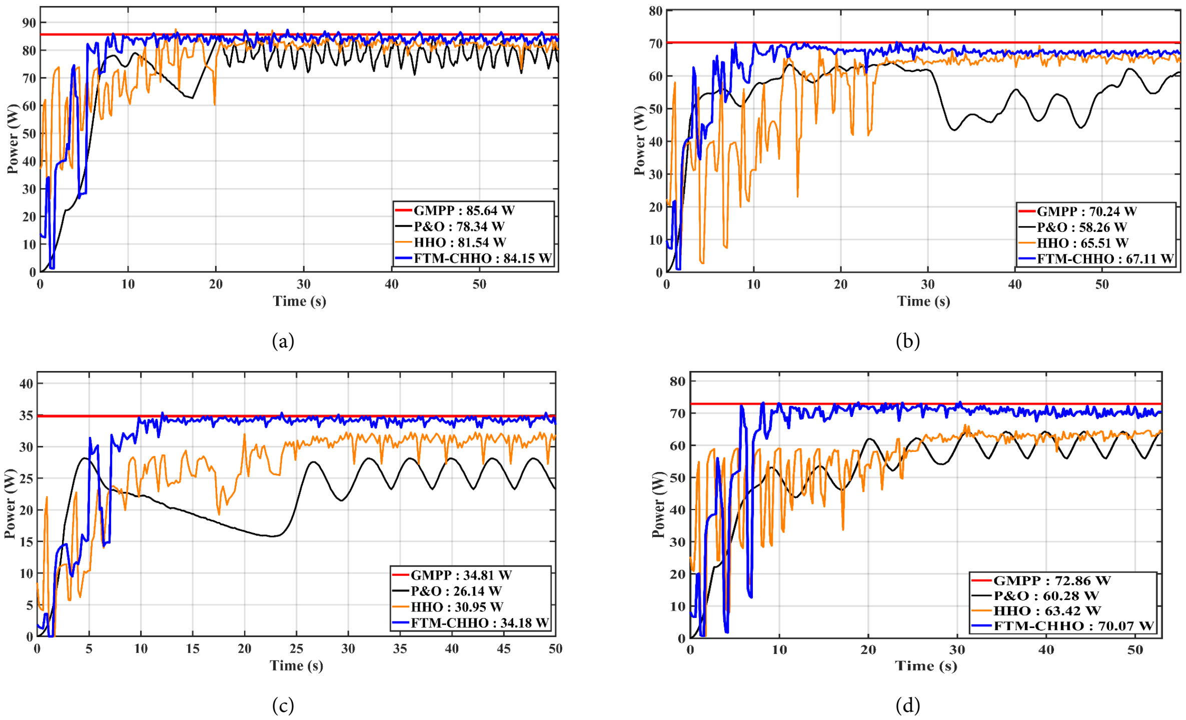

Figure 14. Experimental hardware tracking results under partial shading: (a) Pattern 2; (b) Pattern 3; (c) Pattern 4; (d) Pattern 5.

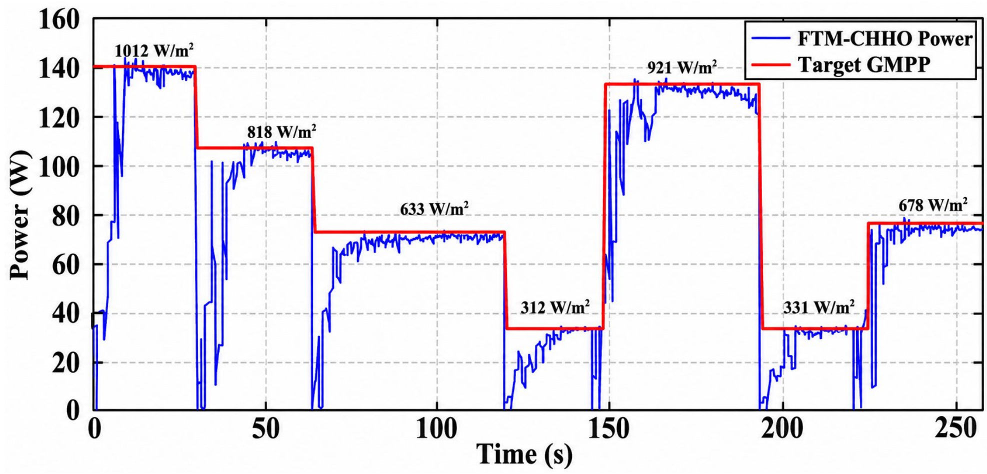

Figure 15. Experimental dynamic tracking performance under varying irradiance conditions.

response demonstrates robust and reliable tracking performance of the proposed method for real-world solar harvesting applications. These findings align with previous studies, where metaheuristic and chaotic-based algorithms successfully tracked the GMPP under partial shading conditions. However, the proposed FTM-CHHO demonstrates improved transient stability and reduced oscillations compared to the standard HHO. Unlike conventional chaotic approaches, the proposed method employs the FTM, which improves ergodicity and reduces early local entrapment. Consequently, FTM-CHHO achieves tracking accuracies between 99.52 % and 100 % with minimal steady-state fluctuations. Similar improvements were also reported in recent literature. Unlike those previous works, this work also includes hardware validation using a SEPIC converter under dynamic irradiance conditions. Although computational complexity increases slightly, FTM-CHHO maintains stable hardware performance. Despite its improved tracking performance, FTM-CHHO still has practical limitations. The integration of fractional calculus and chaotic mapping requires higher computational resources than conventional methods such as P&O. Therefore, real-world implementation requires adequate processing capability (such as 32-bit ARM Cortex architectures) to prevent execution delays during the high-frequency sampling of the SEPIC converter.

IV. Conclusion

This paper proposes and validates the FTM-CHHO algorithm for MPPT under partial shading conditions. By integrating a fractional-order memory mechanism with chaotic maps, the FTM-CHHO reduces premature convergence at local maxima and improves the global search process. Experimental and simulation evaluations, encompassing both simulations and hardware experiments, demonstrate the advantages of the proposed method over the conventional P&O and the standard HHO algorithms. In the simulation phase across five diverse shading configurations, the FTM-CHHO achieved a tracking accuracy ranging from 99.52 % to 100 %, with convergence times between 0.32 s and 0.62 s. In contrast, the P&O algorithm frequently failed due to local entrapment, yielding power extraction efficiencies as low as 66.12 %. The hardware implementation corroborated the simulation findings. Under physically induced partial shading, the FTM-CHHO consistently maintained a high tracking accuracy between 95.54 % and 98.26 %, while reducing the convergence time to under 10.1 s. This performance demonstrates improved tracking capability over the standard HHO, which required longer tracking times up to 27.1 s, and the P&O, which suffered an accuracy drop to 75.09 %. Ultimately, the integration of fractional calculus and chaotic maps provides a robust and precise MPPT solution, supporting effective solar energy harvesting under complex environmental fluctuations.

Acknowledgements

The authors wish to express their sincere gratitude to Politeknik Elektronika Negeri Surabaya (PENS), specifically the Power Electronics for Energy Conversion Laboratory, for providing the essential hardware facilities and technical environment requisite for conducting this experimental research. Furthermore, the authors deeply appreciate the valuable support and contributions from all colleagues and individuals who assisted throughout the preparation of this manuscript.

Declarations

Author contribution

R.P. Eviningsih & **E.A. Irwansyah**: Conceptualization, Methodology, Software, Hardware Implementation, Investigation, Data Curation, Formal analysis, Writing - Original Draft. **E. Sunarno**: Supervision, Project administration, Conceptualization, Writing - Review & Editing. **M.Z. Efendi** & **N.A. Windarko**: Validation, Writing - Review & Editing. **A.T. Nugraha**: Visualization. All authors read and approved the final manuscript.

Funding statement

This research did not receive any specific grant from funding agencies in the public, commercial, or not-for-profit sectors.

Competing interest

The authors declare that they have no known competing financial interests or personal relationships that could have appeared to influence the work reported in this paper.

The use of AI or AI-assisted technologies

During the preparation of this work the authors used Gemini AI in order to check the English grammar, correct typographical errors, and improve the overall readability of the manuscript. After using this tool/service, the authors reviewed and edited the content as needed and takes full responsibility for the content of the publication.

Additional information

Reprints and permission: information is available at https://mev.brin.go.id/.

Publisher's Note: National Research and Innovation Agency (BRIN) remains neutral with regard to jurisdictional claims in published maps and institutional affiliations.

References

[1] M. Y. Worku, M. A. Hassan, L. S. Maraaba, M. Shafiullah, M. R. Elkadeem, M. I. Hossain, and M. A. Abido, "A comprehensive review of recent maximum power point tracking techniques for photovoltaic systems under partial shading," *Sustainability*, vol. 15, no. 14, p. 11132, 2023.

[2] T. Sutikno, A. Pamungkas, G. Pau, A. Yudhana, and M. Facta, "A review of recent advances in metaheuristic maximum power point tracking algorithms for solar photovoltaic systems under the partial-shading conditions," *Indones. J. Sci. Technol.*, vol. 7, no. 1, pp. 131–158, Apr. 2022.

[3] M. S. Endiz, G. Gökkuş, A. E. Coşgun, and H. Demir, "A review of traditional and advanced MPPT approaches for PV systems under uniformly insolation and partially shaded conditions," *Appl. Sci.*, vol. 15, no. 3, p. 1031, 2025.

[4] M. H. Zafar *et al.*, "A novel meta-heuristic optimization algorithm based MPPT control technique for PV systems under complex partial shading condition," *Sustain. Energy Technol. Assess.*, vol. 47, Art. no. 101367, 2021.

[5] M. Agdam, M. J. Morshed, A. Ghasemi, and A. S. Menhaj, "A novel algorithm MPPT controller based on the herd horse optimization for photovoltaic systems under partial shadow conditions," *Eng. Res. Express*, vol. 6, no. 3, Art. no. 035308, 2024.

[6] A. Refaat, A. Kalas, A.-E. Khalifa, and M. H. Elfar, "A comparative study of two metaheuristic MPPT techniques to extract maximum power from PV array under different partial shading patterns," in *Proc. 2023 IEEE Conf. Power Electron. Renew. Energy (CPERE)*, pp. 1–6, 2023.

[7] M. Z. Efendi, A. Adnaurrosyid, M. N. Habibi, R. P. Eviningsih, N. A. Windarko, and M. P. Jati, "MPPT algorithm based on modified remora optimization algorithm for photovoltaic systems under partial shading conditions," *J. Mechatronics, Electr. Power, Veh. Technol.*, vol. 16, no. 2, pp. 204–219, 2025.

[8] N. Akhiriyanto and R. M. Afandi, "Design and implementation of a synchronous buck DC–DC converter with incremental conductance MPPT for green hydrogen production via PEM electrolysis," *J. Mechatronics Electr. Power Veh. Technol.*, vol. 16, no. 2, pp. 220–232, Dec. 2025.

[9] F. Fahmizal, M. R. Sahiddin, P. Herlambang, G. N. Sentana, and H. Maghfiroh, "Design and implementation of a DC-DC buck converter with Type III compensator control," *J. Mechatronics Electr. Power Veh. Technol.*, vol. 16, no. 2, pp. 256–265, 2025.

[10] S. C. Kok, M. Yu, and V. J. Chin, "Design and implementation of a low-cost single-ended primary-inductor converter (SEPIC) for enhanced maximum power point tracking in a photovoltaic system," in *Proc. Int. Conf. Green Energy, Comput. Intell. Technol. (GEn-CITy 2024)*, pp. 163–173, 2024.

[11] P. Megantoro, J. S. Dona Saya, M. A. Syahbani, M. Fadhilah, and P. Vigneshwaran, "Modelling and simulation of maximum power point tracking on partial shaded PV based-on a physical phenomenon-inspired metaheuristic algorithm," *Indones. J. Electr. Eng. Comput. Sci.*, vol. 39, no. 3, pp. 1923–1937, 2025.

[12] S. Sarwar, M. Hafeez, M. Javed, A. Asghar, and K. Ejsmont, "A horse herd optimization algorithm (HOA)-based MPPT technique under partial and complex partial shading conditions," *Energies*, vol. 15, no. 5, Art. no. 1880, 2022.

[13] A.-W. Ibrahim, M. A. M. Ramli, H. Albasri, M. H. Habaebi, M. M. Othman, A. H. M. Yatim, and H. M. Hasanien, "A high-speed MPPT based horse herd optimization algorithm with dynamic linear active disturbance rejection control for PV battery charging system," *Sci. Rep.*, vol. 15, no. 1, Art. no. 3229, 2025.

[14] R. Abbassi and S. Saidi, "Design of a novel chaotic horse herd optimizer and application to MPPT for optimal performance of stand-alone solar PV water pumping systems," *Mathematics*, vol. 12, no. 4, Art. no. 594, 2024.

[15] D. Yousri, T. S. Babu, D. Allam, V. K. Ramachandaramurthy, E. Beshr, and M. B. Eteiba, "Fractional chaos maps with flower pollination algorithm for partial shading mitigation of photovoltaic systems," *Energies*, vol. 12, no. 18, Art. no. 3548, 2019.

[16] M. Al-Dhaifallah, A. M. Nassef, H. Rezk, and K. S. Nisar, "Optimal parameter design of fractional order control based INC-MPPT for PV system," *Sol. Energy*, vol. 159, pp. 650–664, 2018.

[17] R. I. Vais, K. Sahay, T. Chiranjeevi, R. Devarapalli, and Ł. Knypiński, "Parameter extraction of solar photovoltaic modules using a novel bio-inspired swarm intelligence optimisation algorithm," *Sustainability*, vol. 15, no. 10, Art. no. 8407, 2023.

[18] I. Sajid, M. U. Jan, M. A. Khan, A. U. Rehman, A. M. Alharbi, A. M. Almaliki, and N. Javaid, "Optimizing photovoltaic power production in partial shading conditions using dandelion optimizer (DO)-based MPPT method," *Processes*, vol. 11, no. 8, Art. no. 2493, 2023.

[19] I. Shams, S. Mekhilef, and K. S. Tey, "Extendable voltage equalizer topology with reduced switch count and MPPT with partial shading detection capability for long Serially connected PV modules," *IEEE Trans. Ind. Appl.*, vol. 58, no. 5, pp. 6459–6470, 2022.

[20] N. Akram, L. Khan, S. Agha, and K. Hafeez, "Global maximum power point tracking of partially shaded PV system using advanced optimization techniques," *Energies*, vol. 15, no. 11, Art. no. 4055, 2022.

[21] G. Kirana, F. Filiana, and H. Aprillia, "GWO controlled SEPIC converter for maximum power point tracking of solar panel," in *Proc. 2022 Int. Conf. Utility Exhib. Energy, Environ. Climate Change (ICUE)*, pp. 1-6, 2022.

[22] H. S. D. A. Tantya, F. Danang Wijaya, and S. P. Hadi, "Maximum power point tracking using differential evolution algorithm on the SEPIC converter for solar panels under partially shaded conditions," in *Proc. 2024 4th Int. Conf. Sci. Inf. Technol. Smart Admin. (ICSINTESA)*, pp. 427–432, 2024.

[23] A. Saha, A. Dutta, S. Mukherjee, and P. Sarkar, "Modelling and design of ANN-based MPPT controller of SEPIC converter for SPV application," in *Proc. 2024 IEEE Int. Conf. Commun., Comput. Signal Process. (IICCCS)*, pp. 1–6, 2024.

[24] F. MiarNaeimi, G. Azizyan, and M. Rashki, "Horse herd optimization algorithm: A nature-inspired algorithm for high-dimensional optimization problems," *Knowledge-Based Syst.*, vol. 213, Art. no. 106711, 2021.

[25] Y. Zhang, J. Lu, C. Zhao, Z. Li, and J. Yan, "Chaos optimization algorithms: A survey," *Int. J. Bifurc. Chaos*, vol. 34, no. 16, Art. no. 2450205, 2024.

[26] W. F. Mbasso, A. Harrison, I. Dagal, P. Jangir, R. Kumar, and Z. Liu, "Fractional calculus-inspired metaheuristic algorithm for solving high-dimensional constrained optimization problems," *Evol. Intell.*, vol. 19, no. 1, Art. no. 2, 2025.

[27] S. Ahmed and N. Bawany, "Impact of popular chaotic maps on population initialization of sailfish optimizer algorithm – an experimental study," *ADCAIJ Adv. Distrib. Comput. Artif. Intell. J.*, vol. 14, Art. no. e32626, 2025.

[28] A. Hassan, O. Bass, and M. A. S. Masoum, "An improved genetic algorithm based fractional open circuit voltage MPPT for solar PV systems," *Energy Reports*, vol. 9, pp. 1535–1548, 2023.

[29] D. Yousri and M. B. Eteiba, "Fractional chaotic ensemble particle swarm optimizer for identifying the single, double, and three diode photovoltaic models' parameters," *Energy*, vol. 195, Art. no. 116979, 2020.